VOL. 18, NO. 21, NOVEMBER 2023 ISSN 1819-6608
ARPN Journal of Engineering and Applied Sciences

www.arpnjournals.com

CHARACTERISTICS STUDY OF SWITCHED RELUCTANCE MOTOR UNDER VOLTAGE CONTROLLER AND CURRENT CONTROLLER STRATEGIES

Mahmoud Shaker, Hussain F. Jaafar and Hayder Mahdi Abdulridha
Department of Biomedical Engineering, College of Engineering, University of Babylon, Iraq
E-Mail: eng.mahmoud.shaker@uobabylon.edu.iq

ABSTRACT

The presented paper is to investigate the characteristics of the switched reluctance motor (SRM) under different types of controllers. For this study, two different control strategies; namely; voltage and current control strategies are considered. The theoretical background of under consideration controllers is reported. The motor structure, model equations, operation principles as well as the power converter topology and operation are carried out in this research. Motor magnetic characteristics such as inductance profile, phase flux linkages, and static torque profile are studied and simulated. Simulation results of motor performance under each controller are presented. Some recommended conclusions about the SRM suitable controller type selection are introduced.

Keywords: switched reluctance motor (SRM), SMR current control, SMR voltage control, modeling of SRM.

Manuscript Received 22 July 2023; Revised 8 December 2023; Published 10 January 2024

1. INTRODUCTION

Nowadays, switched reluctance motors (SRMs) attract more and more attention [1]. They are simple to construct. SMR consists of two main parts; namely, a stator with excitation windings salient pole and a salient pole rotor without conductors or magnets so the machine rotor among all electrical machines rotor, the salient pole rotor, makes it the simplest rotor possible. Then the characteristics of construction simplicity, low rotor inertia and then high torque- inertia ratio, ease in repairing, and independence between phases with high degree, which gives high performance operation of SMR and so become a challenge for certain industrial applications by finding the way to the electrical drives market. It has been used in battery powered vehicles due to its high efficiency and controllability [2]. Its high speed is suitable for fans, pumps, and certain types of cutting tools. On the other hand, SMR suffers from a few drawbacks, such as some ripple in the produced torque in addition to the acoustic noise which is the most critical [3].

In comparison, the construction with double-salient causes the ripple current in the DC supply to be quite large, so it is required a high filter capacitor.

The absence of permanent magnets causes an excitation load on the stator windings and DC/ AC converter, where the converter KVA requirements increase. To predict the motor performance it is always necessary to solve a set of nonlinear differential equations representing the SRM and its converter. The torque developed by the motor is related to the rotor position, and phase current, and is also affected by the saturation of partially overlapping rotor poles and stator [4, 5]. On the other hand, the average torque can be calculated using integration along the period of rotation [5].

The main challenge of the motor characteristics analysis and control performance depends on the nature of relationships between the flux linkage and the current of each phase winding at different rotor displacement angles. The magnetic saturation to be handled is frequently high, resulting in severe nonlinearity in flux linkage/current curves. The flux linkage/angle relationships cannot generally be taken either as linear or as sinusoidal functions. Many researchers have used the numerical finite element integration method to determine the static phase flux linkage and torque [6, 7, 8]. Alternatively, other analysis methods are used [9, 10]. Many control strategies have been applied to SRM to perform certain objectives such as torque ripple minimization, energy optimization, and sensor less control... etc [11] [12].

In the field of SRM control methods, two widely used basic control methods are used, namely voltage and current control. [14]. In both methods, the objective is a square fundamental waveform, a square voltage waveform in voltage control, and a square current waveform in current control. The square waveform will only be applied in a certain interval, roughly the pole arc [14, 15, 16]. Traditionally the amplitude of the square waveform is controlled by pulse-width-modulation (PWM) in the magnetizing period from α_{on} to α_{off}. In the demagnetizing period from α_{off} to the time when the current or flux becomes zero, the applied voltage is negative and normally not chopped. The reason why the demagnetizing period is done without chopping is to simplify the control-algorithm and improve the SRMs efficiency. With current or voltage control it is possible to control the average torque, but the speed is still uncontrolled. To control the speed, which is a must in modern drives, a speed controller is required. In literature, many different speed controllers have been proposed. In [1] a speed controller of an 8/6 SRM based on a simplified model (linear model) has been introduced. In [17] an 8/6 SRM provided with an optimized harmonic injection technique for speed regulation has also been proposed.

In the present paper, a 2D OPERA version 1.6 finite element analysis method is applied to predict the motor's magnetic characteristics. Two different control strategies are considered. The first is known as the voltage control strategy whereas the other is known as the current control strategy. The theoretical background of under consideration controllers is reported. The motor structure, model equations, operation principles as well as the power converter topology and operation are carried out in this research. Motor magnetic characteristics such as inductance profile, phase flux linkages, normal force, and static torque profile are studied and simulated. Simulation results of motor performance under each controller are presented. Some recommended conclusions about the SRM suitable controller type selection are introduced.

2. MATHEMATICAL MODEL OF SRM

Normally when it is required to derive the SMR equivalent circuit, the mutual inductance per phase is ignored and so the per phase stator current follows the following expression,

$$v_{ph} = iR + \frac{d\lambda}{dt} \tag{1}$$

Where Vph, *i*, R are the DC input DC voltage, the instantaneous phase current, and the resistance of phase winding, while λ represents the linkage of coil flux. The SRM normally operates into saturation to obtain the maximum utilization of the magnetic circuit [3, 13], and so, λ is considered as a nonlinear function of rotor position and stator current, then

$$\lambda = \lambda(i,\theta) \tag{2}$$

The voltage of each phase of the stator can be expressed as:

$$v_{ph} = iR + \frac{\partial\lambda}{\partial i}\frac{di}{dt} + \frac{\partial\lambda}{\partial\theta}\frac{d\theta}{dt} \tag{3}$$

Using the following expression:

$$L(\theta,i)\, i = \lambda(\theta,i) \tag{4}$$

The voltage equation can be rewritten as:

$$v_{ph} = iR + L(\theta)\frac{di}{dt} + i\frac{dL(\theta)}{dt}\omega \tag{5}$$

The right hand terms of Eq. (5) represent the resistive, inductive, and back EMF voltages respectively

Then, the overall instantaneous torque equation for SRM may be obtained using the energy principle Eq. (6):

$$T_{ph}(\theta,i) = \frac{\partial W'(\theta,i)}{\partial\theta}, \qquad i = const. \tag{6}$$

Where W is defined as the energy generated and can be found by:

$$W' = \int_0^i \lambda(\theta,i)\, di \tag{7}$$

Since the torque varies with the time, so the motor global instantaneous torque can be found by summing the torque generated of each phase, i.e.:

$$T_{inst}(\theta,i) = \sum_{phases} T_{ph}(\theta,i) \tag{8}$$

Where T_{inst} represents the instantaneous total torque and Tph is the torque generated by the individual phase.

If it is assumed that the inductance varies according to the rotor position for a given phase current, then the electromagnetic torque of the motor can be expressed as,

$$T_{em} = \frac{1}{2} i^2 \frac{dL(\theta,i)}{d\theta} \tag{9}$$

The motor average torque can be calculated using Eq.(8) as shown in the expression below:

$$T_{av} = \frac{1}{T}\int_0^T T_{inst}\, dt \tag{10}$$

The average air gap power is expressed as:

$$P_a = T_{av} * \omega \tag{11}$$

The electromagnetic developed torque T_{em} and the torque on the motor shaft T_{shaft} are related to each other according to Eq. 12.

$$T_{shaft} = T_{em} - J_{motor}\frac{d\omega}{dt} - T_{fri} \tag{12}$$

where *Jmotor* represents the motor moment of inertia, while ω is the motor angular velocity, and *Tfri* represents the torque losses because of friction.

So the model expression that represents the load considered in this research is given below:

$$T_{load} = J_{load}\frac{d\omega}{dt} + c\omega^2 + b\omega + \tau_{static} \quad (13)$$

where b and c in Eq. (13) are some constants.

To derive the SRMR mechanical model is simply equating equations (12) and (13) that is,

$$T_{em} = J_{total}\frac{d\omega}{dt} + c\omega^2 + b\omega + T_{fri} + \tau_{static} \quad (14)$$

where *Jtotal* is the moment of inertia of both load and motor.

The SRM is intended to operate in deep magnetic saturation [3]. Due to saturation effects and varying reluctance, flux linkage characteristics of the motor appears to be a nonlinear function of both stator currents and rotor position, much like the electrical torque produced. A 2D OPERA version 1.6 finite element analysis methods (FEA) is applied to predict the motor magnetic characteristics. The results of the (FEA) are shown in Figures (1-3).

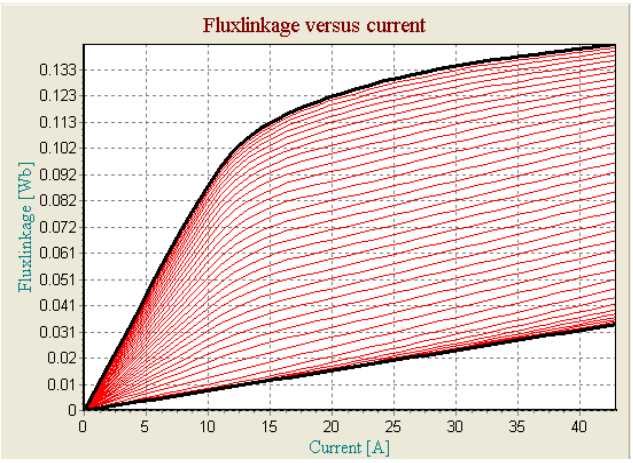

Figure-1. Flux linkage vs. phase current.

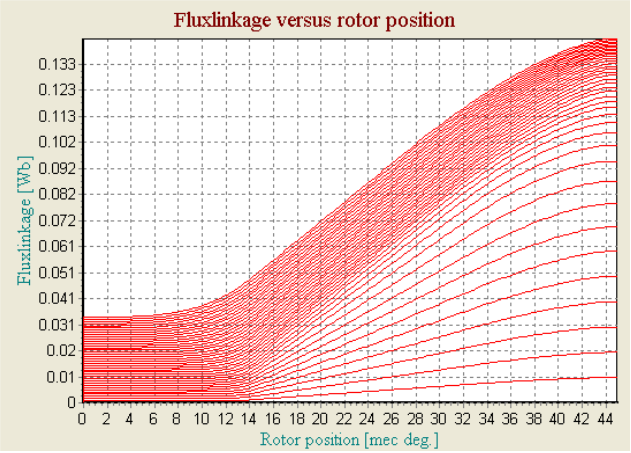

Figure-2. Flux linkage vs. rotor position.

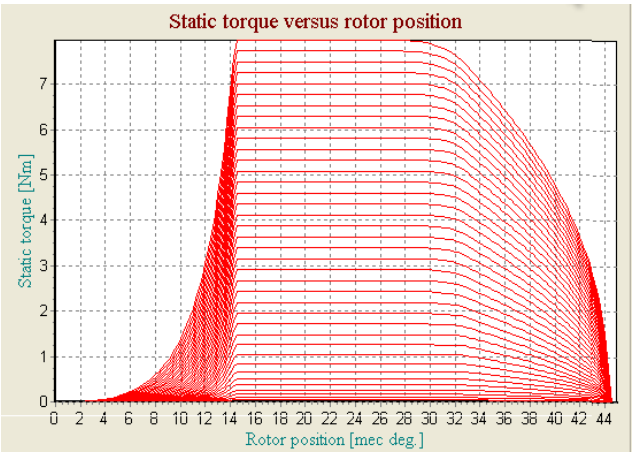

Figure-3. Static torque vs. rotor position.

3. THE INVERTER CIRCUIT

The power inverter circuit used for the present system is shown in Figure-5 the inverter circuit is formed by three asymmetric bridges (one for each phase winding). Each bridge contains two semiconductor switches and two fast recovery diodes. Each phase winding is connected to the midpoints of the two bridge arms. The conduction (or fluxing) period of a certain phase (phase A) is initiated by switching on its higher and lower switches (S11 and S12). If a voltage of positive supply is applied to the phase winding the current will flow through it. At the end of this period, both switches are turned-off to terminate their conduction. The stored energy forces the current to continue flowing through the feedback diodes (D11 and D12) applying a negative supply voltage to the winding (de-fluxing period). When all the stored energy is recovered, the current decays to zero and the diodes are turned-off leaving the phase winding out of duty at zero voltage (dead zone) until the next stroke, this is achieved when (S11 and D11) or (S12 and D12) are conducting. The operating modes and phase (A) voltage, current as well as the switches conduction intervals for such inverter are shown in Figure-6.

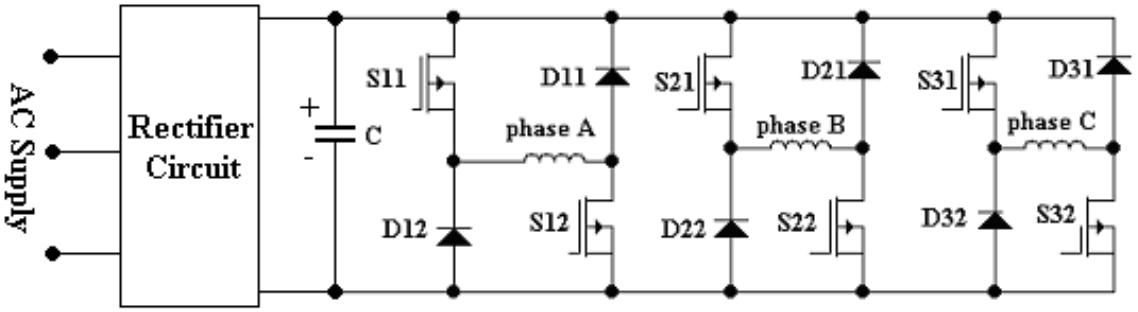

Figure-4. Asymmetric H-bridge inverter.

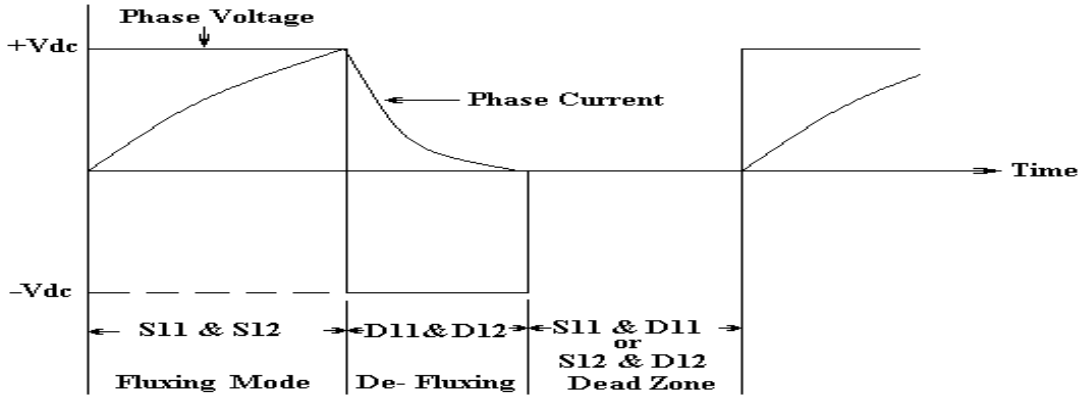

Figure-5. Operating modes of H-Bridge Inverter.

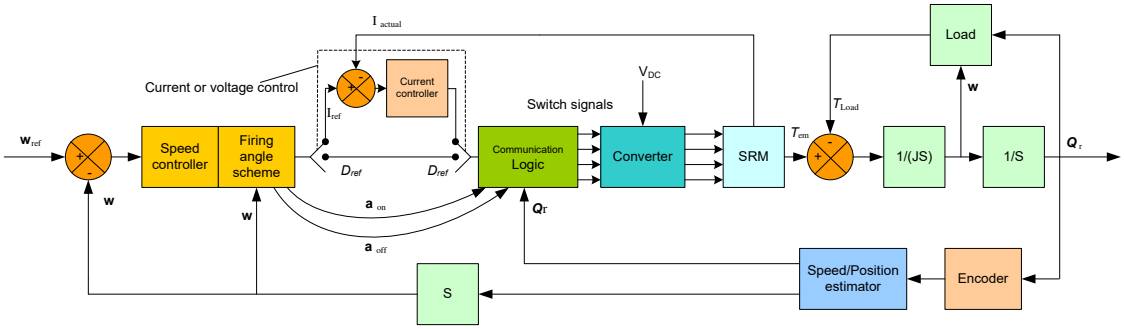

Figure-6. SRM basic control structure.

4. SYSTEM DESCRIPTION AND OPERATION

The block diagram of the controlled system structure considered in the presented is shown in Figure-6. The reference speed w_{ref} is the required speed to which the motor operated. The error signal which is the difference between the reference speed and the actual speed w_{act} which is the feedback signal generated by the speed sensor attached to the motor. The speed sensor is a digital sensor represented by the incremental encoder. A proportional-integrator (PI) controller is used to obligate the motor to operate at the required reference speed. The controller output signal is used as an input signal to the electronic circuit which is responsible for the generation of the necessary firing angle signals to control the operation of the inverter power switches. So, the conditioning circuit of firing commutation angles αon and αoff is determined from the actual speed or the basic chopping parameter (*Iref* or *d*).

In this scheme, it is possible to operate under the two possible chopping modes of operation either with current or with voltage control cases. In current control, the current reference; which represents the output of the speed controller; and the actual current both are subtracted to give the current error. The current error is then used in the current controller. The output from the current controller is like the voltage controller a duty-cycle. This duty cycle is fed to the commutation logic. The function of the commutation logic is to control the converter power switches such that a positive voltage waveform only is applied in the interval from αon to αoff whereby the commutation logic requires knowledge of the rotor position. The converter is fed from a DC-bus voltage

across a capacitor. The outputs from the inverter are PWM-chopped voltages to each phase winding. The developed electro-mechanical torque from the SRM is used to drive the load.

4.1 Current Control Strategy

A traditional strategy to control the current of the SRM is the hysteresis current control, where the semiconductor switches are switched on and off depending on the reference current *Iref* and Hysteresis band ΔI. Both hard chopping and soft chopping may be used to change the state of the switches [15, 17]. In hard chopping, current increases by a large factor typically (5-10 times), and for this reason, it is not desirable as a control strategy for motoring operations [15]. In this paper, only soft chopping is used.

4.2 Voltage Control Strategy

In the case of the voltage control method, the voltage amplitude is controlled by controlling the duty cycle (d) of the inverter switches. In the magnetizing time of operation (turn-on mode) the duty cycle must be more than zero and remain at constant value till reaches the case in which the turn-off angle happened. After that, a rapid demagnetization case in the phase happens by applying a complete negative voltage on its terminals.

A single pulse control mode of operation is also known as a single pulse control mode of operation if the duty cycle is set to its maximum value (d=1) [3, 5, 15, 16].

Then, there are three modes of operation are considered; namely: turn-on angle mode, turn-off mode, and the single mode operation.

5. RESULTS AND DISCUSSIONS

The present paper deals with the basic control strategies of the SRM. The study is applied to a three-phase 6/4 SRM whose ratings and specifications are given in the appendix. The study is carried out for different speed operations starting from 3000 rpm to 6000 rpm. Selected results at two extreme speed operations (3000 rpm and 6000 rpm) are shown in figures (7-10). While Figures (7, and 8) show the motor characteristics under the current control method at 3000 rpm and 6000 rpm respectively, the motor characteristics under the voltage control strategy are respectively shown in Figures (9, and 10). Motor performance such as output power, torque ripple, efficiency, and losses are performed and compared in Figure-11 for current and voltage control strategies. At low speed operation i.e. at (3000 rpm), the motor does not have sufficient impedance or back-EMF to limit the current raising. So the two main strategies to be applied are the closed loop current regulation (hysteresis current control) and the PWM voltage control as shown in Figures (7, and 9). From Figure-7a it is obvious that the current raising is very rapid at the instant of switching-on the power converter switch because of the small backing EMF, but as the speed is increased, the current is kept close to the reference current from αon to αoff . As shown, the controller maintains a flat current waveform with a small ripple until the commutation angle αoff. After that point (Figure-7 a, b)) the phase flux linkage must be reduced rapidly to ensure that no negative torque zone is generated. Figures (7c and 9c) show the energy conversion loops at 3000 rpm. In contrast to Figures (8c and 10c); which represent the energy conversion loops at 6000 rpm; the phase flux linkage reached a high level, this is attributed to the small inductance variations at this low speed. The average torque can be obtained by integrating the area between the aligned and unaligned positions over a whole period of rotation. The electromagnetic torque developed by the motor at 3000 rpm is respectively shown in Figures (7d and 9d) for current and voltage control. About these two figures, the developed torque is almost the same, except that a high torque ripple is developed in the voltage-controlled SRM (175% instead of 126% for current controlled SRM at the same speed of operation). Even though the current controlled SRM gives a relatively lower torque ripple compared to the voltage-controlled SRM at the same speed of operation, the torque ripple is increased in the current controlled SRM at very low speeds of operation, this may attributed to the high switching frequency which leads to high ripple and high losses that deficiency the whole drive at this low speed (Figure-11).

At higher speeds the motor EMF increases to a level at which there is insufficient voltage available to regulate the current (due to the high voltage drop across the converter elements), then the torque can only be controlled by timing the current pulses, i.e. the single-pulse control mode or firing angle control mode. In this mode of operation, the duty cycle becomes unity in the whole conduction period (in the voltage control) and the current reference becomes higher than the current limited by the back-EMF (in current control). This can be seen in Figures (8 and 10) when the motor entered this mode of operation. In these figures, the motor performance is almost the same except that the torque ripple generated by the voltage-controlled SRM is relatively higher than that generated by the current controlled SRM. From Figure-11 it can also be observed that the phase current draws in the current controlled SRM are relatively higher than that of voltage-controlled SRM, which relatively increases the total torque, but at the expense of motor efficiency.

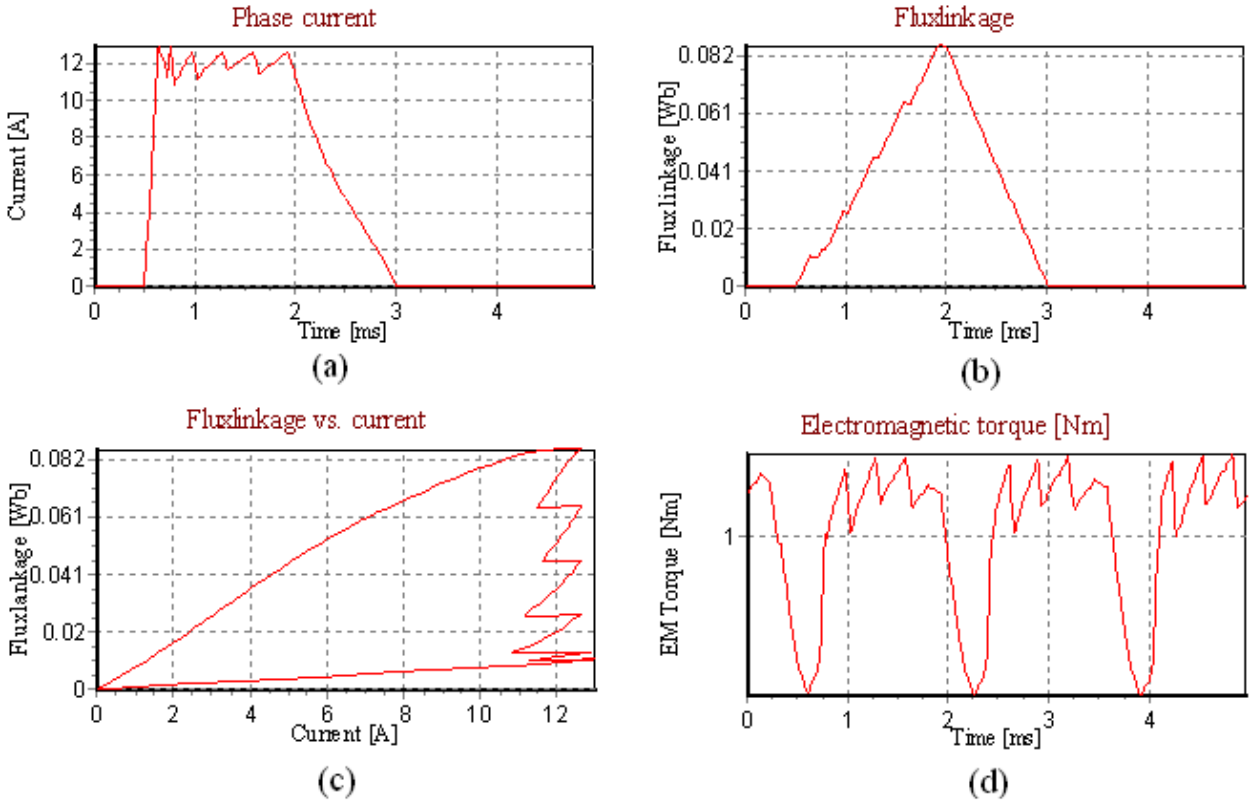

Figure-7. SRM performance at 3000 rpm and Current Control (a) phase current vs. time, (b) phase flux linkage vs. time, (c) flux linkage vs. current and (d) Electromagnetic torque vs. time.

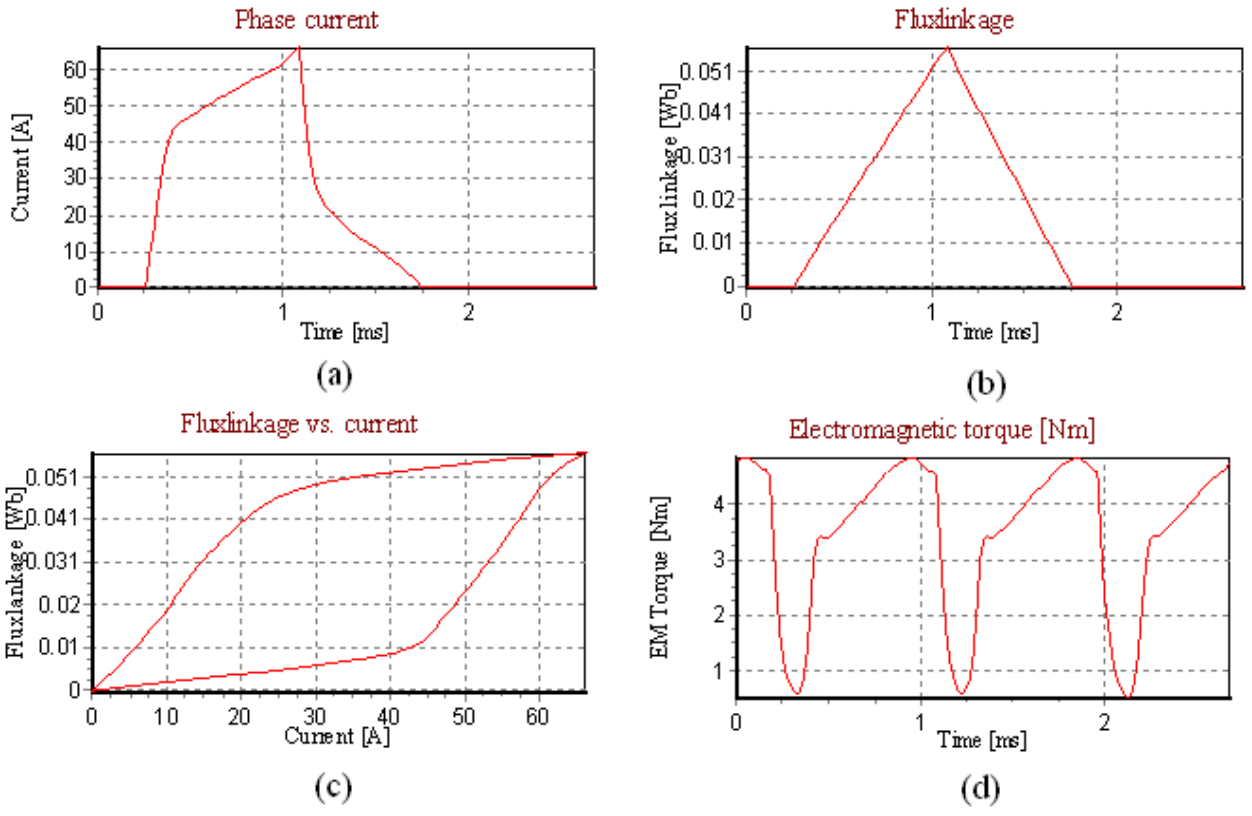

Figure-8. SRM performance at 6000 rpm and Current Control (a) phase current vs. time, (b) phase flux linkage vs. time, (c) flux linkage vs. current and (d) Electromagnetic torque vs. time.

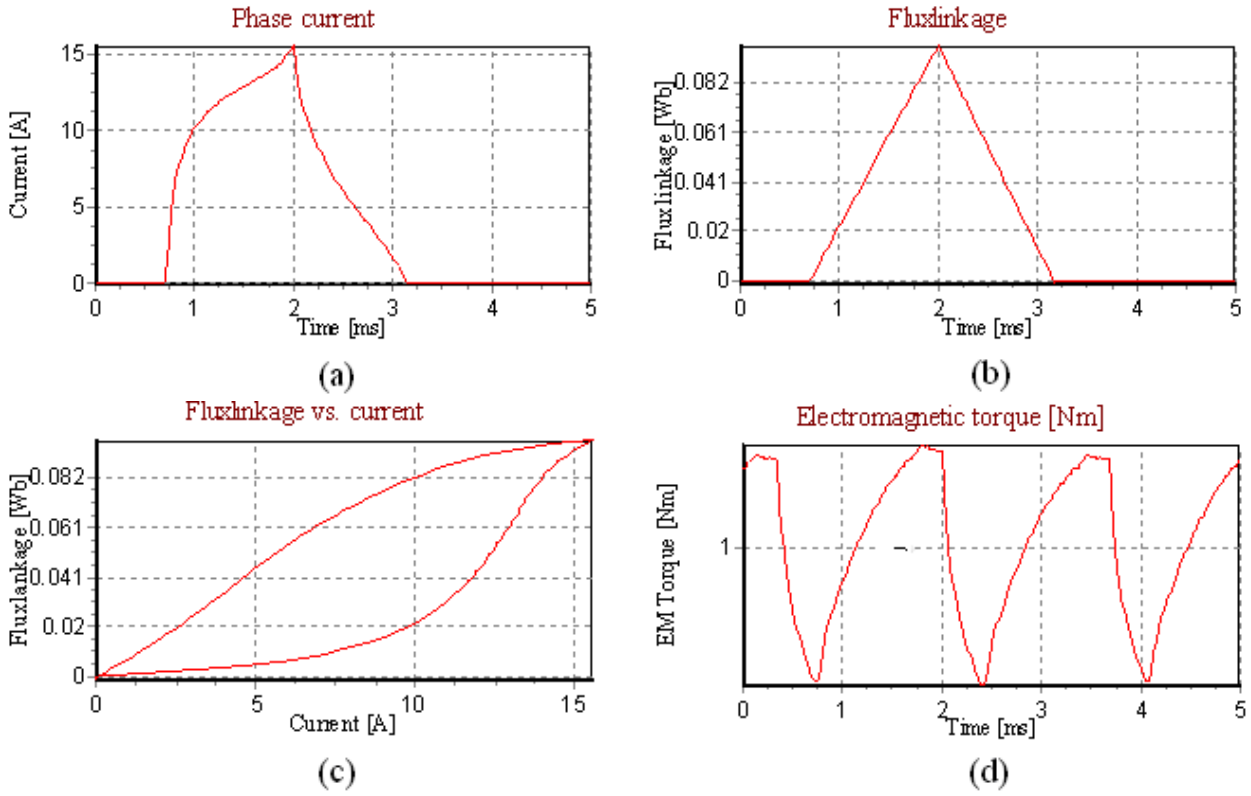

Figure-9. SRM performance at 3000 rpm and Voltage Control (a) phase current vs. time, (b) phase flux linkage vs. time, (c) flux linkage vs. current and (d) Electromagnetic torque vs. time.

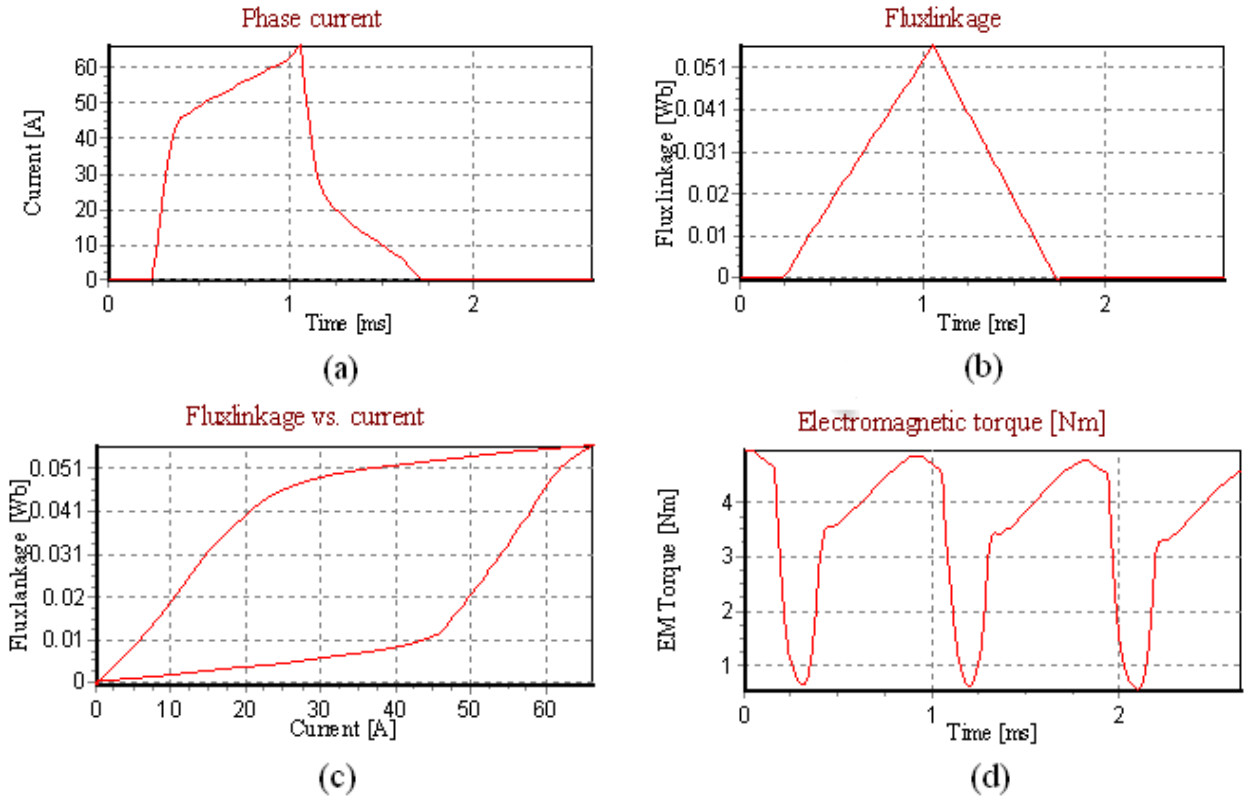

Figure-10. SRM performance at 6000 rpm and Voltage Control (a) phase current vs. time, (b) phase flux linkage vs. time, (c) flux linkage vs. current and (d) Electromagnetic torque vs. time.

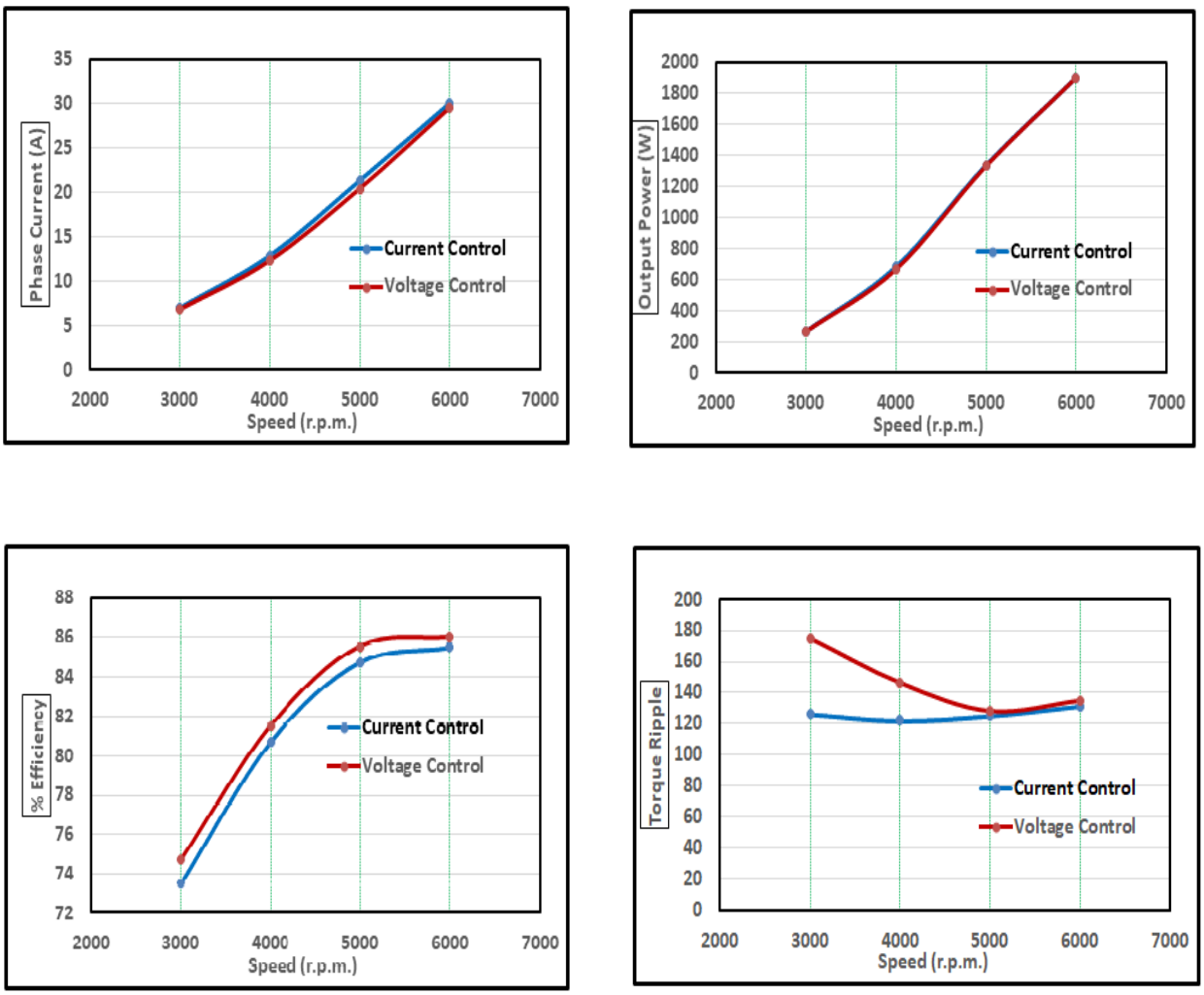

Figure-11. A comparison of motor performance at different speeds.

6. CONCLUSIONS

In this paper, a simulation study has been carried out to investigate the basic control strategies of the SRM. Two different basic control strategies have been implemented. The first is known as the voltage control strategy whereas the other is known as the current control strategy. Motor performance under each control strategy is investigated and good correlations have been obtained. From the present study, it has been observed that the current control strategy is suitable for medium and high speeds of operation. The restriction to using the current control strategy for medium and high speeds is that the torque ripple generated by the current controlled SRM at low and very low speeds of operation is relatively high, which leads to increasing the total losses and decreasing the efficiency of the whole system. To avoid such problems current controlled SRM provided with an advanced turn-on angle technique may be applied. Simulation results have also shown that the voltage-controlled SRM is feasible at low speeds. This may attributed to low switching losses at this low speed, which leads to increasing the efficiency at the expense of the produced torque.

Appendix

Motor ratings and specifications:

The 6/4 three-phase SRM used in this paper has ratings and specifications listed in the table below:

Quantity	Value
No. of Stator poles (Ns)	6
No. of Rotor poles (Nr)	4
Dc link voltage [V]	80
Nominal speed [rpm]	2500
Max. Speed [rpm]	8000
Rotor pole arc [°m]	31.50
Stator pole arc [°m]	29.90
Airgap length [mm]	0.25
Inductance ratio	11.441
Rotor inertia [kg.m²]	0.001
Shaft radius [mm]	7
Power[KW]	2

The load

The load driven by the SRM has the following dynamic equation:

$$T = J\frac{d\omega}{dt} + C\omega^2 + B\omega + \tau_{Static}$$

where:
B= 1e -4 [1/nm]
C= 1e -5 [1/nm²]
τstatic= 0.001 [nm].

List of symbols

d	= duty cycle
R	= per phase stator resistance
Iref	= reference current
Δ I	= hysteresis band
v	= phase voltage
is	= phase current
L	= phase inductance
λ	= phase flux linkage
θ	= rotor position
ω	= rotor speed in rad/sec
Tph	= phase torque
W'	= the co-energy
αon	= switch turn-on angle
αoff	= switch turn-off angle
PWM	= pulse width modulation
Tinst	= instantaneous torque
Tem	= electromagnetic torque
Tav	= average torque
Pav	= average airgap power

REFERENCES

[1] D. C. Dursun, A. Yildiz and M. Polat. 2022. Modeling of Synchronous Reluctance Motor and Open and Closed Loop Speed Control. 2022 21st International Symposium INFOTEH-JAHORINA (INFOTEH). pp. 1-6.

[2] M. A. Abdulatif, S. Tahoun, M. Khater, M. El-Shnawany and S. Hassan. 2000. Dynamic Performance of Four Pole per Phase 12/8 Switched Reluctance Motor. Engineering Research Bulletin, 23(1), Minufiya University, Faculty of Engineering, Egypt.

[3] Iqbal Husain. 2002. The Power Electronics Handbook. edited by T. I. Skvarenina, Industrial Electronics Series, Purdue University, Indiana.

[4] S. Suresh, J. Peter and V. Chellappan. 2022. Mathematical Modeling and Speed Control of 6/4 Switched Reluctance Motor Drive. 2022 International Conference on Futuristic Technologies in Control Systems & Renewable Energy (ICFCR). pp. 1-6.

[5] Berker Bilgin, James Weisheng Jiang and Ali Emadi. 2019. Switched Reluctance Motor Drives: Fundamentals to Applications. 1st Edition, CRC press, Taylor & francis Group, ISBN 13: 978-1-1383-0459-8.

[6] J. Rizk, M. Nagrial, and A. Hellany. 2003. Design Optimization of Switched Reluctance Motors. Technical paper, Institution of Engineers, Australia.

[7] G. Urgera, B. C. Mecrow, M. Michon, X. Deng and M. Popescu. 2022. 3D Effects in Static Flux-linkage Characterization of Switched Reluctance Drives. *2022* International Conference on Electrical Machines (ICEM). pp. 1082-1088.

[8] J. Lindsay, R. Arumugam and R. Krishnan. 1986. Finite Element Analysis Characterization of a Switched Reluctance Motor with Multitooth per Stator Pole. IEE, proc. Vol. 133.

[9] A. Omekanda and M. Renglet. 1997. Calculation of the Electromagnetic Parameters of a Switched Reluctance Motor using an Improved FEA-BIEM-Application to Different Models for the Torque Calculation. IEEE trans. on Indus. Applications. 33(4).

[10] Daniel Marcsa and Miklos Kuczmann. 2016. Finite element analysis of switched reluctance motor with rotor position based control. Pollack Periodica. 11(3): 153-164.

[11] Funda Sahin, H. Bülent Ertan and Kemal Leblebicioglu. 2000. Optimum Geometry for Torque Ripple Minimization of Switched Reluctance Motors. IEEE, trans. on energy conv. 15(1).

[12] G. Singh and B. Singh. 2020. An Analytical Approach for optimizing Commutation Strategy of Switched Reluctance Motor Drive for Light Electric Vehicle. 2020 IEEE International Conference on Power Electronics, Smart Grid and Renewable Energy (PESGRE2020). pp. 1-6.

[13] W. Wu, J. Dunlop, S. Collocott and B. Kalan. 2003. Design Optimization of Switched Reluctance Motor by Electromagnetic and Thermal Finite-Element Analysis. IEEE, trans. on magnetic. 39(5).

[14] P. Omand. 2001. Design and Advanced Control of Switched Reluctance Motors" PhD dissertation, Aalborg University.

[15] T. J. E. Miller. 1993. Switched Reluctance Motors and Their Control. Magna Physics Publications, Oxford UK, ISBN 1-881855-02-3.

[16] T. J. E. Miller. 2001. Electronic Control of Switched Reluctance Machines. Newnes Power Engineering Series, ISBN 0-7506-50737.

[17] Yun Zhang, *et al*. 2022. Speed Control of Switched Reluctance Motor Based on Regulation Region of Switching Angle. Energies, 2022, 15, 5782, MDPI, Basel, Switzerland.